



The spatial morphology of Europa's near-surface O₂ atmosphere

T.A. Cassidy^{a,*}, R.E. Johnson^a, M.A. McGrath^b, M.C. Wong^c, J.F. Cooper^d

^a *Engineering Physics Program and Astronomy Department, University of Virginia, P.O. Box 400325, Charlottesville, VA 22904-4325, USA*

^b *NASA Marshall Spaceflight Center, VP01, Huntsville, AL 35812, USA*

^c *Jet Propulsion Laboratory, 4800 Oak Grove Drive, Pasadena, CA 91109, USA*

^d *Heliospheric Physics Laboratory, Code 672, NASA Goddard Space Flight Center, Greenbelt, MD 20771, USA*

Received 10 January 2007; revised 24 April 2007

Available online 24 May 2007

Abstract

Results from a three-dimensional ballistic model of Europa's O₂ atmosphere are presented. Hubble Space Telescope (HST) ultraviolet observations show spatially non-uniform O₂ airglow from Europa. One explanation for this is that the O₂ atmosphere is spatially non-uniform. We show that non-uniform ejection of O₂ alone cannot reproduce the required morphology, but that a non-uniform distribution of reactive species in Europa's porous regolith can result in a non-uniform O₂ atmosphere. By allowing O₂ molecules to react with Europa's visibly dark surface material, we produced a spatially non-uniform atmosphere which, assuming uniform electron excitation of O₂ over the trailing hemisphere, compares favorably with the morphology suggested by the HST observations. This model, which requires a larger source of O₂ than has previously been estimated, can in principal be tested by the New Horizons observations of Europa's O₂ atmosphere.

© 2007 Elsevier Inc. All rights reserved.

Keywords: Europa; Regoliths; Satellites, atmospheres; Satellites, surfaces

1. Introduction

Europa's tenuous O₂ atmosphere was predicted to exist due to magnetospheric plasma bombardment by Johnson et al. (1982). Energetic magnetospheric ions and electrons produce the O₂ by radiolytic decomposition of water ice (Johnson, 1990). The O₂ atmosphere was first detected via Hubble Space Telescope (HST) observations of atomic oxygen emissions at 1304 and 1356 Å (Hall et al., 1995, 1998). The ratio of the 1304 to 1356 Å emission line intensities implied that the emissions come from electron impact dissociation of O₂, and not from electron impact excitation of atomic oxygen. Hall et al. (1995, 1998) derived a disk averaged vertical column density of 2.4×10^{14} – 1.4×10^{15} O₂/cm² for the trailing hemisphere observations assuming both a uniform atmosphere and a spatially uniform electron impact excitation rate.

A subsequent HST observation of the trailing hemisphere of Europa found that the oxygen emission was spatially non-

uniform, with the brightest emission above the Northern Bright Plains (McGrath et al., 2004; and described in the next section), a region that may have unusually pure water ice (Domingue and Hapke, 1992; Fanale et al., 1999). Cassini observations by Hansen et al. (2005) also suggested that Europa's atmosphere may be spatially and/or temporally non-uniform.

Interpreting the spatially non-uniform emission requires an understanding of both the electron flux and the O₂ density distribution. The Saur et al. (1998) model of electron flow around Europa suggested a non-uniform electron density and temperature. However, their atmospheric model did not reproduce the non-uniform emission seen by the HST; instead, it predicts a nearly radially symmetric emission for the geometry of that observation (Fig. 19.10 in McGrath et al., 2004). The model also predicts that the electron density and temperature are anti-correlated. Since the O₂ electron-impact dissociation cross section increases with electron energy in the relevant temperature range (Kanik et al., 2003), the effect of electron density on O₂ dissociation efficiency is partially canceled by the variation in electron temperature. Therefore, in attempting to describe the HST observations we consider only the spatial non-uniformity of the O₂ atmosphere.

* Corresponding author.

E-mail address: tac2z@virginia.edu (T.A. Cassidy).

With the assumption that the spatial non-uniformity seen in the HST image is due solely to a spatially non-uniform O_2 atmosphere, we will show that the required atmosphere *cannot* be created only by non-uniform O_2 ejection produced, for example, by a non-uniform distribution of the incident plasma. This is the case because O_2 does not condense onto water ice at the relevant surface temperatures and its lifetime against ionization or dissociation is long (~ 6 Earth days). Thermally desorbing O_2 molecules moving randomly between the atmosphere and the icy surface travel an average horizontal distance of about 2000 km in that time. Therefore, unless there is some additional loss process, the O_2 atmosphere generated by a non-uniform O_2 source produces a nearly uniform global O_2 atmosphere (Shematovich et al., 2005). In this paper we explore the effect of spatially variable surface/ O_2 reactivity on the morphology of the O_2 atmosphere.

Telescopic and spacecraft images of Europa show that its surface composition is spatially inhomogeneous. Sulfur and carbon-containing species have been detected in the ice matrix, as summarized by Johnson et al. (2004), providing possible reaction sites for O_2 . O_2 might also become trapped more efficiently in an ice with impurities such as SO_2 and CO_2 , which are known components of the darker surface regions (Hand et al., 2006). While sustained exposure to O_2 might be expected to eventually quench the reactivity, intense bombardment by Jupiter's magnetospheric plasma breaks chemical bonds in the surface material (Carlson et al., 1999; Cooper et al., 2001), providing new opportunities for O_2 to react. This issue is discussed further in Section 7. After briefly reviewing the HST observations we first describe the effect of a reactive surface on the returning O_2 and then use those results to construct atmospheric emission images for comparison with the HST observations.

2. HST observations

The HST observation of Europa in Fig. 1 was obtained on 5 October 1999 using the Space Telescope Imaging Spectrograph (STIS) with grating G140L (~ 1100 – 1700 Å) and the

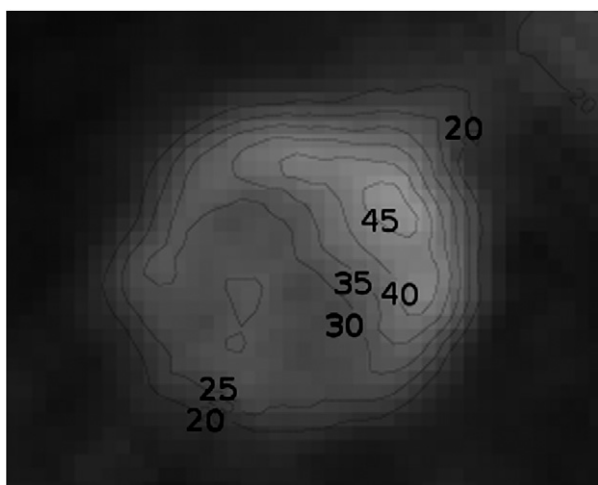


Fig. 1. The 1999 HST STIS observation of Europa's O_2 atmosphere. The image is a line emission at 1356 Å resulting from the electron-impact dissociation of O_2 . The contours show calculated column density in units of $10^{14} O_2 \text{ cm}^{-2}$.

Table 1
Summary of observations

Exposure #	Start time	Exposure time (s)	Orb./west. long.	Sys III	Notes
o5d61dyq		0.30			Acquisition image
o5d601010	08:39:27	830	244.8	303.9	
o5d601020	08:56:45	830	246.0	313.1	High bck
o5d601030	09:59:01	1100	250.6	347.5	
o5d601040	Failed				Failed
o5d601050	11:35:41	1100	257.4	39.0	
o5d601060	11:57:29	1100	258.9	50.6	
o5d601070	13:13:03	1100	264.3	90.8	
o5d601080	13:34:51	1100	265.8	102.5	
o5d601090	14:49:04	1100	271.0	142.0	
o5d6010a0	15:14:37	1100	272.8	155.6	

$52'' \times 2''$ slit. Five orbits of HST time were used with 2 exposures performed in each orbit. A standard CCD acquisition was performed before the science observations. Because Europa's $1.08''$ diameter is smaller than the slit width used, the observations effectively provide objective spectra and monochromatic images of the satellite in the oxygen and hydrogen emission lines. The observations occurred while Europa was near dusk (western) elongation and spanned orbital and system III longitudes of 245° – 273° and 290° – 150° , respectively, during the course of the observations. The phase angle was $\sim 4^\circ$ throughout the observation. By definition the orbital longitude is equal to sub-HST west longitude, so Fig. 1 shows mainly the trailing hemisphere (apex at west longitude 270°), which is also the sunlit hemisphere. A summary of the observation is presented in Table 1. We have extracted the monochromatic image of Europa in the OI 1356 Å emission line from each observation, and summed all the exposures because the signal to noise ratio is less than one in the individual exposures. The S/N of the summed image is ~ 2 . The summed image, converted to column density, is shown in Fig. 1. The conversion to column density assumes that the electron density and temperature are constant along the line of sight, and uses a rate coefficient for dissociative excitation of O_2 leading to 1356 Å emission of $1.1 \times 10^{-9} \text{ cm}^3 \text{ s}^{-1}$, after Hall et al. (1998).

When interpreting the morphology of UV emission, the lifetime and speed of the excited O atoms that result from O_2 dissociation must be considered. For the 1356 Å emission the excited O lifetime is $180 \pm 5 \mu\text{s}$ (Nowak et al., 1978), and for 1304 Å, $1.82 \pm 0.05 \text{ ns}$ (Lawrence, 1970), while the O atoms have speeds around 3 km s^{-1} (Smyth and Marconi, 2006). Thus the UV emission essentially occurs at the site of O_2 dissociation, so collisional quenching with other gas species or the ground is insignificant.

3. Effect of surface reactivity

We will now demonstrate the effect of reactive species on the O_2 density above the surface for various test parameters using a ballistic Monte Carlo atmospheric model. For this section and Fig. 2, Europa's surface is assumed to be non-porous. The implications for a porous regolith are discussed in the next section. The Monte Carlo model follows about 10^5 test parti-

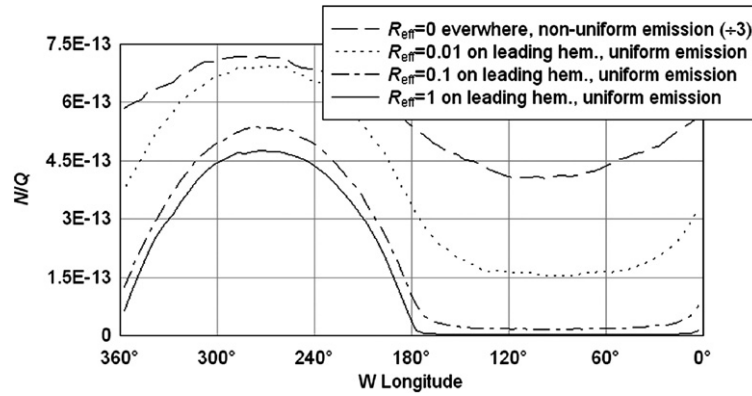


Fig. 2. Latitude-averaged O₂ scaled vertical column density (N/Q , column density divided by total O₂ source rate) above Europa's surface for different test models. Topmost dashed line: O₂ ejection from the trailing hemisphere only (180° to 360° west longitude) and no surface reactivity ($R_{\text{eff}} = 0$ everywhere). All other lines were calculated for uniform O₂ ejection from Europa's entire surface, but with nonuniform reactivity: $R_{\text{eff}} = 0$ on the trailing hemisphere, $R_{\text{eff}} = 1, 0.1$, or 0.01 on leading hemisphere, as indicated by the legend.

cles to represent O₂ molecules, and uses these test particles to calculate column densities. Ejection points are distributed randomly across Europa's surface with some probability distribution. Each O₂ test particle is ejected with a kinetic energy chosen via a Monte Carlo procedure from the sputtering energy distribution

$$\frac{dP}{dE} = \frac{U}{(E + U)^2}, \quad (1)$$

where $(dP/dE)dE$ is the probability of ejecting a molecule with a kinetic energy between E and $E + dE$, and $U = 0.015$ eV. This distribution is a fit to a laboratory measurement of O₂ formed and ejected by heavy-ion bombardment of pure water ice (Brown et al., 1984). The small fraction (less than 1%) of O₂ molecules that reach Europa's Hill sphere boundary at 8.7 Europa radii are assumed to escape. The exit-angle distribution is assumed to be given by

$$\frac{dP}{d\cos(\theta)} = 2\cos(\theta), \quad (2)$$

where θ is the angle of ejection from Europa's local surface normal (Cassidy and Johnson, 2005).

The ejected O₂ molecules are then followed on ballistic trajectories until they return to Europa's surface. It is assumed that the atmosphere is collisionless, even though the Hall et al. and McGrath et al. column densities are near the limit of the definition of an exosphere. The no-collision assumption is therefore at the edge of applicability, but collisions will affect our results only marginally. All other components of the atmosphere, including sputtered H₂O, have densities at least several orders of magnitude lower than O₂ and should not affect this approximation (Hall et al., 1998; Shematovich et al., 2005).

The O₂ molecules returning to Europa's surface are transiently adsorbed, a process called physisorption. While adsorbed, they can migrate to a reaction site or, at Europa's surface temperatures, be thermally desorbed. The probability of reaction is denoted by R_{eff} . If a reaction occurs the O₂ is no longer tracked. The notation R_{eff} is used to distinguish the reactivity of a porous regolith from that of a non-porous laboratory

surface, whose reactivity is denoted by R . The relationship between R_{eff} and R is discussed in the next section. In our Monte Carlo model, the O₂ molecules that do not react are assumed to desorb immediately as their residence time on water ice at the relevant temperatures is typically very short compared to ballistic flight times (Shi et al., 2007). The kinetic energy of thermally desorbed O₂ molecules is determined by the Maxwell flux distribution, which is the Maxwell-Boltzmann distribution multiplied by velocity and normalized. This distribution has an average kinetic energy of $2k_bT$, where T is the local surface temperature and k_b is Boltzmann's constant.

The desorbed O₂ then follows another ballistic trajectory and the process is repeated until the O₂ either reacts with the surface or is lost to space. We assume that the loss to space occurs everywhere at the rate of $1.9 \times 10^{-6} \text{ s}^{-1}$. There is some uncertainty in this number, but varying it, even by an order of magnitude, has a negligible effect on our simulations due to the dominance of surface reactivity as a loss process. The number chosen ($1.9 \times 10^{-6} \text{ s}^{-1}$) is an estimate of the electron-impact ionization (Saur et al., 1998; McGrath et al., 2004). Another loss process of similar magnitude is electron-impact dissociation (Smyth and Marconi, 2006). Thus the O₂ lifetime is much longer than the ballistic flight time, and because most O₂ molecules are desorbed many times before loss, the majority of O₂ molecules present in the atmosphere were ejected from the surface by thermal desorption (Ip et al., 1998; Shematovich et al., 2005). The Saur et al. (1998) model of Europa's O₂ atmosphere suggested that atmospheric sputtering is the dominant O₂ loss process, but Shematovich et al. (2005), using a 1-D atmospheric model, found that this loss process is much smaller than the electron impact ionization rate. Saur et al. (1998) assumed that all ion/O₂ collisions are head-on (zero impact parameter) and elastic. Such a collision imparts a large momentum to the target O₂ molecules; so much so that every collision will result in the escape of an O₂ molecule unless its trajectory intersects the surface. If a range of impact parameters is allowed, only a small portion of all the ion/O₂ collisions will result in an O₂ molecule with enough energy to escape.

In order to calculate the O₂ column density we assume that the atmosphere is in steady state, i.e., $dN/dt = 0$, where N is

the O₂ column density. The rate of change of the number of particles, N , in a column of area A is calculated from test particle trajectories. It is a balance between particles entering the column and those exiting: $dN/dt = fQ/A - N/\Delta t_{av}$, where Δt_{av} is the average time spent in the column, Q is the O₂ source rate and f is the fraction of the ejected O₂ that enter the column. In steady state, $N = fQ\Delta t_{av}/A$. Generalizing to a distribution of particle sources and speeds, the column density is

$$N = \frac{w \sum \Delta t_i}{A}. \quad (3)$$

Here Δt_i is the time that test particles spend in the column of interest and w is the test particle weight. The test particle weight is given by Q/M , where Q is the number of O₂ molecules ejected per unit time from Europa's entire surface and M is the number of test particles used in the model. The test particle weight has units of inverse time. It is clear that N is directly proportional to Q , the total O₂ source rate. Therefore, our calculated column densities N can be scaled by Q , in which case they have units of cm⁻² s. This method of calculation applies to both vertical and line-of-sight column density. *Vertical* column density is the number of O₂ per unit area above Europa's surface, while *line-of-sight* column density is the number of O₂ per unit area along the line of sight extending from HST to Europa.

The steady-state assumption is complicated by Europa's rotation. This complication is partially avoided by calculating column densities in a reference frame rotating with Europa. In this frame the surface features, of course, do not move. Likewise, because Europa is tidally locked to Jupiter, the mean plasma flow direction relative to the surface features is nearly constant. Some flow variations do arise from tilt of the jovian planetary magnetic dipole axis relative to the rotation axis. The surface temperature, however, is not constant in a rotating reference frame, which we discuss in the next section. For the test models discussed in this section, including Fig. 2, we use a globally uniform and constant 100 K surface temperature.

The ballistic trajectory calculations neglect Jupiter's gravity. The only forces acting on the O₂ particles are Europa's gravity and, implicitly, via Europa's rotation, the Coriolis force. Tiscareno and Geissler (2003) discussed the effect of Jupiter's gravity on the trajectories of sputtered H₂O, and found it to be small. The effect of Jupiter's gravity on O₂ trajectories is even smaller, since most of the O₂ in Europa's atmosphere has been thermalized, and so has a small scale height of about 20 km (Ip et al., 1998; Shematovich et al., 2005; Smyth and Marconi, 2006).

Fig. 2 (topmost dashed line) demonstrates the consequences of non-uniform O₂ ejection and no surface/O₂ reactivity or sticking. In this model O₂ was sputtered (using Eq. (1)) uniformly from the trailing hemisphere (no sputtering on the leading hemisphere), and $R_{eff} = 0$ everywhere. The latitude-averaged vertical column density displayed was divided by Q . Because the primary O₂ loss process, electron impact ionization, is a slow process, with a time constant of ~6 days, repeated thermal desorption allows the O₂ to spread across the surface.

The other lines in Fig. 2 were calculated using uniform sputtering of O₂ from the entire European surface, but with non-uniform surface/O₂ reactivity: $R_{eff} = 0$ on the trailing hemisphere and $R_{eff} = 1.0, 0.1$, or 0.01 on the leading hemisphere. The hemispheric vertical column density dichotomy is seen to be much larger even for a small surface reactivity than in the case of non-uniform ejection and no surface reactivity. The O₂ column density is, not surprisingly, inversely correlated with R_{eff} . The O₂ distributions in Fig. 2 are not meant to be realistic. Their purpose is to demonstrate the efficacy of using a non-uniform R_{eff} to create a non-uniform atmosphere. A model with realistic parameters is described in a later section.

4. Effect of regolith porosity

Europa's surface is covered by a porous regolith (Domingue and Verbiscer, 1997). Because of the porosity, the probability of a reaction between an O₂ molecule and Europa's regolith (R_{eff}) can be much larger than the probability of a single regolith grain/O₂ reaction (R). This is analogous to the comparison of effective surface albedo to the single-scattering albedo of grains in the regolith described in Hapke (1981). To calculate R_{eff} we used the Monte Carlo model described by Cassidy and Johnson (2005) to estimate sputtering and photodesorption yields when those processes take place within a regolith. The net yield was shown to depend on the probability that an ejected species permanently adsorbed or reacted on regolith grains, which we described as a 'sticking coefficient' for the sputtered ejecta. The sticking coefficient, as used in that paper, described the probability of *permanent* adsorption of a molecule onto a regolith grain. Thus, for the purposes of this paper, the reaction probability R is interchangeable with the sticking coefficient (S) used by Cassidy and Johnson (2005) because both describe the probability of permanent loss. For instance, H₂O sticks with a probability of ~1 at Europa's temperature and so would, in this model, have $R = 1$.

To calculate R_{eff} we assumed that the regolith grains are spherical, and that the sputtering ions and returning O₂ molecules are uniformly incident (i.e., the flux to the surface is proportional to the cosine of the incident angle). The angular distributions of sputtered and thermally desorbed ejecta with respect to the regolith surface grain normal were assumed to be both given by Eq. (2) and the sputtering yield as a function of an ion's angle of incidence g onto the regolith-grain surface is given by $Y(g=0) \cos(g)^{-x}$, where $Y(g=0)$ is the sputtering yield at normal incidence and x is a number between 1 and 2. These last two expressions are empirical formulae for ejection of O₂ from water-ice sputtering experiments (Johnson, 1990). It is assumed that the regolith grains are locally flat so that such experimental results can be used.

We found that the porosity of the regolith can considerably enhance R_{eff} as compared to that for a flat, smooth surface. The reason for this enhancement is that an O₂ molecule returning to Europa's regolith does not interact just once with the surfaces of grains but interacts many times, with the average number of interactions being a function of R . The effective reactivity, as shown in Fig. 3, can be approximated by the following least-

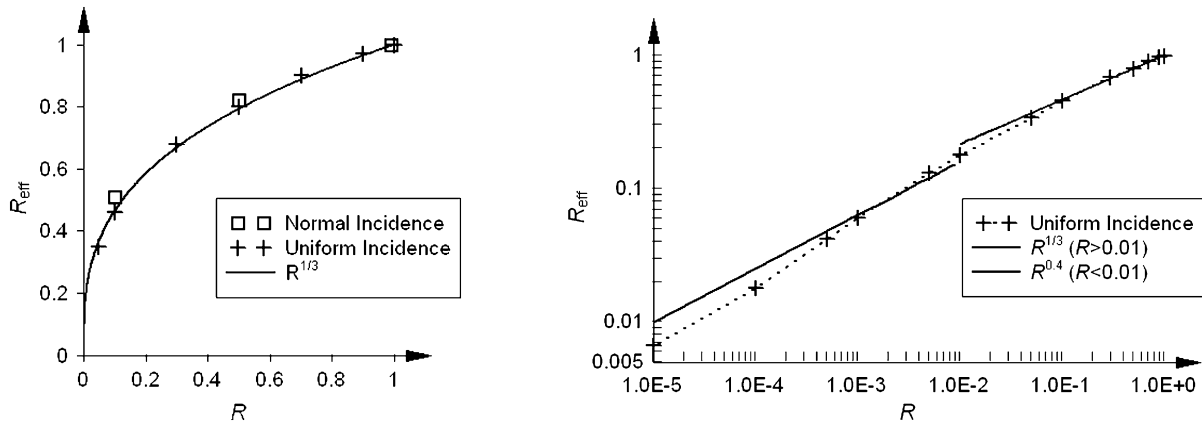


Fig. 3. Effective reaction probability (R_{eff}) for a regolith made up of grains with surfaces that have a reaction probability R . Left panel (linear scale): data points are results from the Monte Carlo model calculations using two different parameter sets; the solid line is the fit $R_{\text{eff}} = R^{1/3}$. Right panel (log–log scale): fit (black lines) to the Monte Carlo results (data points joined by dashed line) over a broad range of R (see Eq. (6)).

squares fit to the Monte Carlo results, which do not depend on the value of x in the expression for the angular dependence above:

$$\begin{aligned} R_{\text{eff}} &= R^{1/3}, & 0.01 \leq R \leq 1, \\ R_{\text{eff}} &= R^{0.4}, & R \leq 0.01. \end{aligned} \quad (4)$$

R_{eff} is always larger than R . For small R , R_{eff} is larger by orders of magnitude. For instance, in Fig. 2 we gave the leading hemisphere of Europa's surface $R_{\text{eff}} = 0.01$. Equation (4) tells us that the probability of an O₂/regolith-grain reaction is $R = 10^{-5}$, i.e., an O₂ molecule would have to interact with grain surfaces, on average, 10^5 times before a reaction with a species in the grain surface occurred.

In the models described in the previous section, the O₂ was sputtered using the energy distribution in Eq. (1). The presence of regolith changes this. Since O₂ is sputtered *within* a regolith, most sputtered O₂ molecules will encounter a regolith grain rather than directly leave the regolith. Those that leave the regolith without encountering a regolith grain have the sputtering energy distribution but those that encounter a grain are either thermally desorbed from that grain or are lost by a reaction with the surface with probability R . Subsequently the O₂ can either leave the regolith or encounter another grain. The overall yields of thermally desorbed and sputtered O₂ are functions of R , as described in Cassidy and Johnson (2005), and are given by the following least-squares fit to the Monte Carlo results where we used $x = 1.6$, which is appropriate for a number of materials:

$$\begin{aligned} Y_{\text{therm}}/Y(g=0) &= 1.68 - 2.13R^{1/3} + 0.36R^2, \\ Y_{\text{sput}}/Y(g=0) &= 0.72, \\ Y_{\text{tot}} &= Y_{\text{therm}} + Y_{\text{sput}}. \end{aligned} \quad (5)$$

Here $Y(g=0)$ is the same quantity mentioned above, the sputtering yield due to ions normally incident onto a smooth flat surface. The subscripts “therm” and “sput” refer to thermalized sputter products and directly ejected sputtering products, respectively. Adding these two equations gives the total sputtering yield scaled to the laboratory value at normal incidence, $Y_{\text{tot}}(R)/Y(g=0)$, which varies between 0.72 and 2.5 if

$x = 1.6$. This incorporates two effects: reactions with grains in the regolith, and the angular enhancement of the yield, which is not well measured for O₂ production. The two effects compete: reactions lower the effective sputtering yield and the variation in the yield with incident angle increases the yield. Since R is small for all of the parameter sets used in the models described in the next section, the angular enhancement has by far the largest effect on sputtering yield.

These results are largely independent of other regolith properties such as regolith grain shape, angular distribution of sputtered ejecta with respect to regolith–grain surface normal, regolith depth, as long as the regolith is deep enough, and porosity, as long as the porosity is high enough. Specifically, the Monte Carlo program was designed with the assumption that the mean free path λ is larger than the average grain width D . For spherical grains and the standard definition of $\lambda = 1/n\sigma$, where σ is the regolith grain cross section and n is the number density of regolith grains, this implies that the model regolith must have a volume fraction of empty space (porosity) greater than 1/3. Europa's porosity has been estimated at between 0.6 to nearly 1.0 (Hendrix et al., 2005).

Cassidy and Johnson (2005) described similar robustness for other regolith effects. An example is given in Fig. 3, where R_{eff} was calculated for normally incident and uniformly incident sputtering ions. Both result in nearly identical expressions for R_{eff} . Because of this robustness, and lack of reference to the specific properties of either O₂ or Europa, Eq. (4) may be applied to any molecule returning to the surface of any body with a sufficiently thin atmosphere [e.g., Na on Mercury as described by Leblanc and Johnson (2003)].

5. O₂ atmosphere model

The Monte Carlo model used to generate Fig. 2 is adapted here to include realistic spatial distributions of the O₂ source rate, surface temperature, and effective surface reactivity to reproduce the 1999 STIS observation, which is shown in Figs. 1 and 4a. The regolith effect of R -dependent sputtering yield (Eq. (5)) is ignored because of the small values for the effective reactivity, R_{eff} , used in the models. As discussed in Section 4,

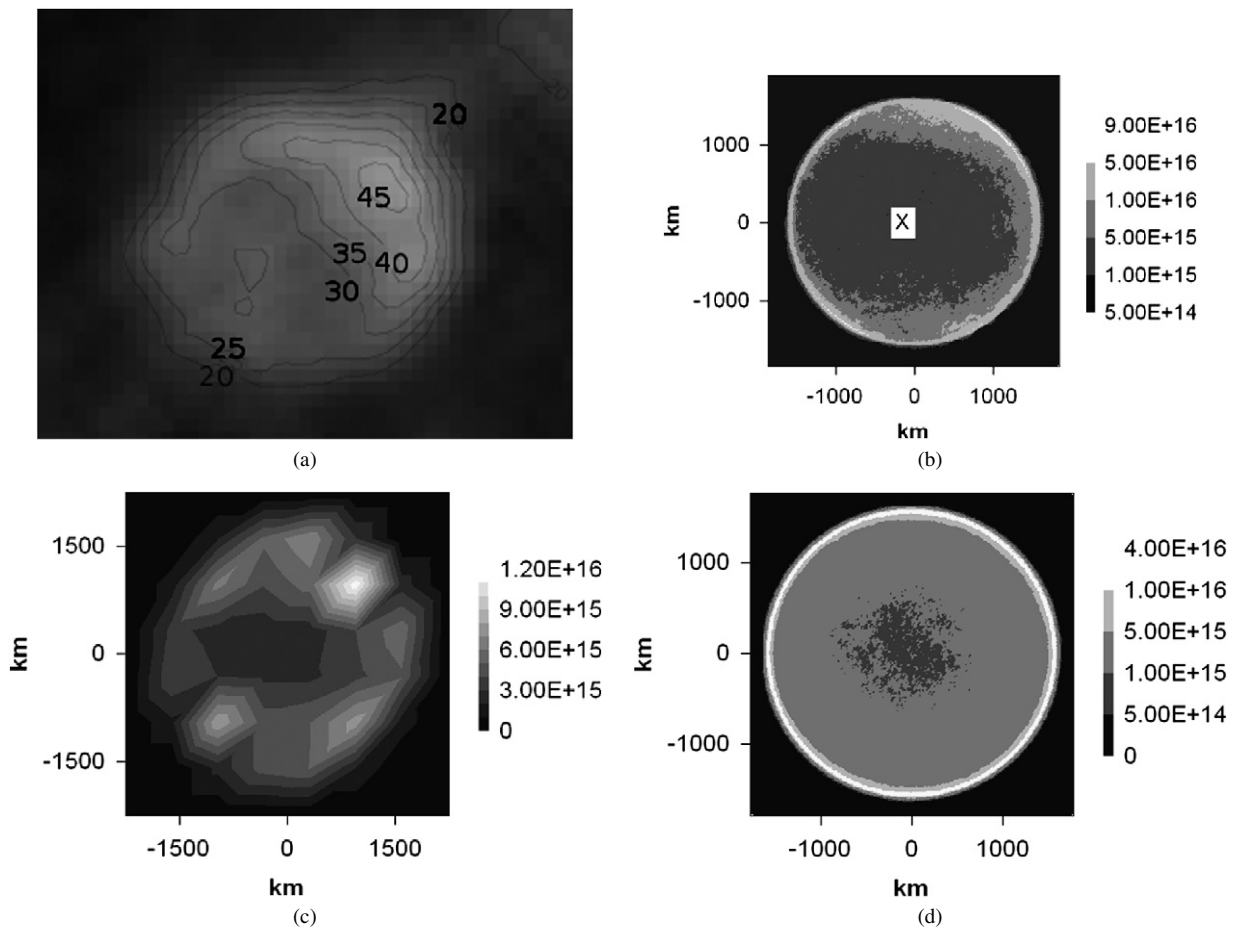


Fig. 4. Line of sight O_2 column density (cm^{-2}). Comparison of model simulations of Europa's O_2 atmosphere and Hubble Space Telescope image of O_2 airglow shown in (a); the contours labels show column density in units of $10^{14} O_2 cm^{-2}$. (b) Case 1: uniform O_2 ejection from Europa's entire surface and reactivity $R_{1,eff} = 0.04$. The average location of the trailing-hemisphere apex is marked by "X." Image resolution 20 km. (c) Same as simulation as (b), but with resolution of 600 km to match the HST STIS resolution. (d) Case 5: preferential O_2 ejection from the icy regions and no reactivity. For clarity, the high resolution (b) and (d) use very different scales than the low resolution (a) and (c), which use linear scales.

the energy distribution of the ejected O_2 is a normalized sum of the sputtering and Maxwell-flux distributions.

Temperatures were obtained from the [Spencer et al. \(1999\)](#) temperature map, which is based on Galileo mission data. The dayside temperature map was fit with the function $40 + 50 \cos(\theta)^{1/4} + 40 \cos(i)$ K, where θ is the latitude and i is the solar zenith angle. The nightside temperature was fit by the function $40 + 50 \cos(\theta)^{1/4}$ K. The errors on the fit were ± 10 K, although actual errors may be larger due to the reasons discussed by [Spencer et al. \(1999\)](#). An accurate temperature distribution is important because, all other parameters being equal, the O_2 column density is anticorrelated with temperature. This effect is not seen in 1-D ballistic atmosphere models, where increasing the surface temperature increases a desorbed particle's speed, and thus particle's ballistic flight time, which increases the column density ([Johnson, 1990](#)). The same is true in our 3-D model, but that effect is overwhelmed by another: O_2 desorbed from a high-temperature region travels farther in its ballistic arc than from a low-temperature region so that, after many desorptions, the average O_2 molecule spends more time in the low temperature region. This result depends on the

low sticking probability of O_2 , and so would not apply to atmospheric components such as H_2O .

The region over which has the largest O_2 emission was seen roughly corresponds to a high-albedo region known as the Northern Bright Plains (NBP) as classified by [Lucchitta and Soderblom \(1981\)](#) using a limited number of high-resolution Voyager images. [McEwen \(1986\)](#) used lower-resolution Voyager images at multiple wavelengths to determine photometric properties of the surface. Based on these he constructed a map covering most of Europa's surface in which terrain was divided into 4 units, with unit 4 roughly corresponding to Lucchitta and Soderblom's bright plains classification, and unit 1 corresponding to impurity-rich dark regions described by, for instance, [Fanale et al. \(1999\)](#) and [Johnson et al. \(2004\)](#). Each unit covers about one quarter of Europa's surface area.

Based on this qualitative correlation between McEwen's unit 4 and the large O_2 emission feature (which, we assume, results from a relatively large O_2 column density), we used [McEwen's \(1986\)](#) map as a proxy for reactivity. McEwen stated that there may be just two units, with units 2 and 3 being a patchwork combination of units 1 and 4, so we gave unit

Table 2
Summary of simulations

Case	O ₂ ejection distribution	Shown in Fig. 4	Successful at reproducing Fig. 4a
1	Uniform	Figs. 4b and 4c	Yes, $Q = 2.0 \times 10^{28}$
2	Preferential ejection from icy regions	Not shown (similar to case 1)	Yes, $Q = 8.3 \times 10^{27}$
3	Preferential ejection from trailing hemisphere (5.5:1 ratio)	Not shown	No
4	Preferential ejection from trailing hemisphere (2:1 ratio)	Not shown (similar to case 1)	Yes, $Q = 1.8 \times 10^{28}$
5	Case 2, no reactivity	Fig. 4d	No

$4R_{\text{eff}} = 0$, gave unit 1 the reactivity $R_{\text{eff},1}$, and gave units 2 and 3 intermediate reactivities $R_{\text{eff},3} = (1/3)R_{\text{eff},1}$ and $R_{\text{eff},2} = (2/3)R_{\text{eff},1}$, where the subscripts refer to the unit classification. The poles above 70° latitude, which were not classified by McEwen, were also given $R_{\text{eff},1}$ to best reproduce the observation, which suggests low column density above the poles (see Fig. 4a). $R_{\text{eff},1}$ was varied to best reproduce the spatial variation of the 1999 STIS observation.

The simulation produces scaled column densities, column density divided by the total source rate, as described in Section 3. The total O₂ source rate Q is an independent parameter; varying Q does not change the spatial distribution. Q (O₂ s⁻¹) times a scaled column density (O₂ cm⁻² s) yields a column density (O₂ cm⁻²). A value for Q was determined by the disk-averaged scaled column density. Q is the number which, when multiplied by the calculated disk-averaged scaled column density, yields the disk-averaged column density measured during the 1999 STIS observation. The simulation results in 4 have been multiplied by Q to show actual column densities.

6. Results

We considered a number of models for Europa's O₂ atmosphere, but only display results for three characteristic cases. These models depend on the spatial morphology of both the O₂ ejection and the effective surface reactivity. Initially we display only the line-of-sight column densities for the portion of the disk observed by HST. The observation (Fig. 4a) is an average over several sub-HST west longitudes (Table 1), so our simulations are each averaged over the same longitudes. The different cases are summarized in Table 2 (Q is the required total O₂ production rate).

For case 1 O₂ is ejected uniformly from Europa's entire surface. It applies when most of the sputtering is done by high-energy ions, which impact the entire surface nearly uniformly, and the O₂ production efficiency is spatially uniform (Paranicas et al., 2002; Pospieszalska and Johnson, 1989). We found that the smallest $R_{\text{eff},1}$ that could roughly reproduce the isolated bright spot from the 1999 STIS observation is $R_{\text{eff},1} = 0.04$. The simulation result is shown in Figs. 4b and 4c, the former with a resolution of 20 km and the latter with a resolution of 600 km to simulate the HST STIS resolution. This low resolution was chosen because the point spread function's full-width

half-max is roughly 4 pixels (Kimble et al., 1998), and each pixel is about 150 km wide at Europa in the 1999 STIS observation. The disk-averaged column density for this calculation is $(1.5 \times 10^{-13} \text{ O}_2 \text{ cm}^{-2} \text{ s})Q$. The 1999 STIS observation found a disk-averaged O₂ column density of $3.0 \pm 1.0 \times 10^{15} \text{ cm}^{-2}$, thus it requires a total O₂ source rate, Q , of $2.0 \pm 1.0 \times 10^{28} \text{ O}_2 \text{ s}^{-1}$.

It is worth noting that the average O₂ lifetime for this case was 5 h, with most O₂ molecules being lost to reactions in the regolith. Since Europa rotates about 21° during 5 h, this means that the temperature distribution does not change dramatically during the simulation and supports our decision to use the steady-state approximation. From Eq. (4), $R_{\text{eff}} = 0.04$ requires $R = 3.2 \times 10^{-4}$. This means that an O₂ molecule on unit 1 terrain adsorbs and desorbs, on average, 3×10^3 times before finding a reaction site.

For case 2, O₂ was ejected preferentially from the icy regions. As an extreme case we gave the dark terrain of unit 1 a sputtering yield of 0. This was implemented by multiplying the test particle weight by a coefficient: 1 if O₂ was ejected from unit 4, 2/3 from unit 3, 1/3 from unit 2, and 0 from unit 1. We found that the smallest $R_{\text{eff},1}$ that could roughly reproduce the HST observation is $R_{\text{eff},1} = 0.01$, and the result is nearly identical to Fig. 4b, so this case is not shown in Fig. 4. The O₂ source rate Q necessary to reproduce the 1999 STIS disk-integrated result is $7.8 \pm 3.7 \times 10^{27} \text{ s}^{-1}$, about a factor of two lower than the previous case. This Q was calculated in the same manner as case 1. From Eq. (4), $R_{\text{eff}} = 0.01$ requires $R = 1 \times 10^{-5}$.

For cases 3 and 4 we used preferential O₂ ejection from the trailing hemisphere. This may occur due to preferential ion (Pospieszalska and Johnson, 1989) or electron (Paranicas et al., 2001) irradiation. To implement such a test model, we used the form in Fig. 1 of Pospieszalska and Johnson (1989), which is similar to the O₂ ejection distribution assumed by Ip et al. (1998). That distribution is approximated here as

$$\frac{dP}{d\cos(\Theta)} = A + B \cos(\Theta)H(\cos(\Theta)), \quad (6)$$

where Θ is the angle with respect to the center of trailing hemisphere (180° opposite the direction of Europa's orbital motion), and H is the Heaviside Step Function. This distribution is a cosine flux on the trailing hemisphere, due to either the corotating plasma or the hot electrons, with the production efficiency determined by B , and a small longitude-independent flux on the leading hemisphere, due to the energetic ions with the production efficiency determined by A . The ratio $B/A \sim 5.5$ corresponds roughly to the ion flux ratio. Using this ratio in Eq. (6) we were unable to find an $R_{\text{eff},1}$ that reproduces the 1999 STIS observation. However, because the slow ions, energetic ions and energetic electrons all have different O₂ production efficiencies, we altered the ratio of A to B . For case 4 we adjusted the ratio to produce a trailing/leading O₂ production ratio of 2.0, and the results are nearly identical to case 1 (Figs. 4b and 4c) if we set $R_{\text{eff},1} = 0.03$.

Finally, for case 5, O₂ is ejected preferentially from the icy regions, as in case 2, but with *no reactivity* anywhere on Europa's surface. This again demonstrates that non-uniform ejection

tion alone is insufficient to produce the 1999 STIS observation. The same is true if the O_2 lifetime against loss to space (ionization or dissociation) is increased or decreased by an order of magnitude. Case 5 is shown in Fig. 4d.

The majority of the O_2 atmosphere is thermal with an extended non-thermal population due to the source distribution in Eq. (1). This is seen in Fig. 5, where the globally averaged density of O_2 as a function of altitude is shown. Below about 200 km the atmosphere falls off exponentially with a scale height of 20 km. Above 200 km the atmosphere is dominated by a non-thermal population, which has an effective scale height ~ 500 km. Similar results were found for the 1-D atmospheric model of Shematovich et al. (2005).

Useful observations were carried out during the encounter of New Horizons with the jovian system. Alice, New Horizons' UV spectrometer, observed Europa's O_2 atmosphere UV emissions at a variety of times and sub-spacecraft longitudes, although only disk-averaged emissions were measured (John Spencer, personal communication). The results presented above

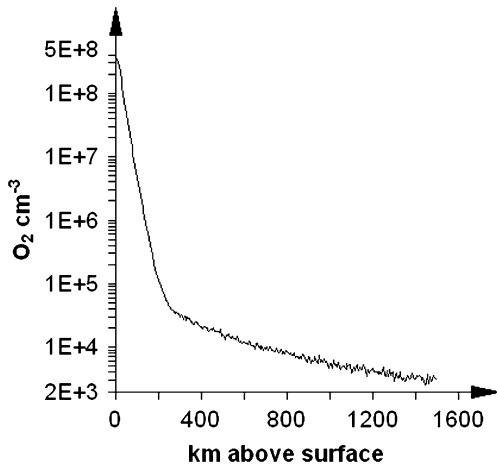


Fig. 5. Globally-averaged O_2 density as a function of altitude for case 1. This shows both the thermalized and much smaller non-thermal O_2 populations.

are based on a single viewing geometry, so in Fig. 6 predictions are made for other viewing geometries. It should be kept in mind, however, that spatial and temporal variations in electron density and temperature (Kliore et al., 1997; Saur et al., 1998) means that the results in Fig. 6 are not directly proportional to atomic oxygen emissions. Further, the reactivity map we used may be inappropriate for the leading hemisphere. The results in Fig. 6 are the normalized disk-averaged line of sight column density as a function of sub-spacecraft longitude for some of the simulations listed in Table 2. These results are little affected by the location of noon ($<5\%$ variation). Three simulations (cases 1, 2, and 4) closely resemble the 1999 STIS observation. Cases 1 and 2 have the highest column density on the leading hemisphere; the ratio of the leading apex/trailing apex disk-averaged line-of-sight column density is a factor of 1.4 and 1.6, respectively. Case 4 has a flat curve, similar to the unsuccessful case 5. Previous simulations predicted different results. For example, Ip et al. (1998) predicted that the highest O_2 column density would be on the trailing hemisphere (similar to case 3). In contrast to this Saur et al. (1998) use a more uniform O_2 column density, but predicted that the atomic oxygen emissions would be larger on the trailing hemisphere due to the “electron cavity” on the leading hemisphere. We note that such a cavity could account for the fact that Hall et al. (1998) and Hansen et al. (2005) both found stronger O emissions from the trailing hemisphere. Their observations of the leading and trailing hemispheres, however, were taken days or weeks apart and the temporal variations seen by Hall et al. (1998) were the same magnitude as the spatial variation. Analysis of the New Horizons observations may allow us to separate the temporal and spatial variation.

7. Summary and conclusions

The 3-D model for Europa's O_2 atmosphere described here shows that a small reactivity in Europa's sulfur-containing ice can dramatically affect the morphology of Europa's O_2 at-

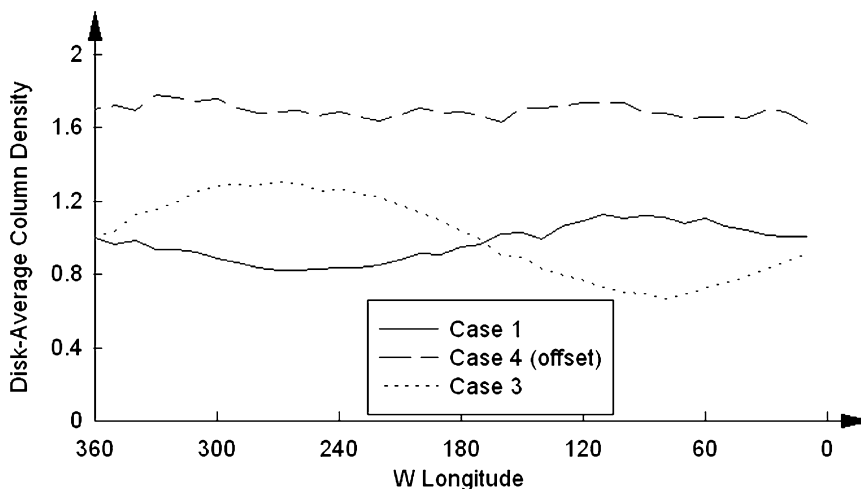


Fig. 6. Normalized O_2 disk-averaged column density at a variety of sub-spacecraft longitudes using the same parameters used for the simulations listed in Table 1, as indicated by the legend. The column density at west longitude 0 was arbitrarily given the value 1, but with one of the curves offset for clarity. The curve for case 1, shown here, is qualitatively similar to the curve for case 2. The curve for case 4, shown here, is qualitatively similar to the curve for case 5. Cases 1, 2, and 4 are the simulations that best reproduce the HST O_2 airglow image.

mosphere. The efficacy of surface reactivity at reproducing the HST observation was demonstrated for a variety of O₂ ejection distributions (see Table 2). By using the global mosaic of McEwen (1986) as a proxy for O₂/surface reactivity we can roughly reproduce the 1999 HST STIS detection of a spatially non-uniform emission feature from Europa's O₂ atmosphere. Only small reactivity is needed because the typical O₂ molecule interacts with a large number of surfaces during its lifetime. The average distance traveled by an O₂ molecule during its lifetime in the successful simulations varies between 500 and 1000 km (depending on reactivity); this number is a rough measure of the sensitivity of the atmosphere to surface feature spatial variation (the average O₂ travels ~2000 km if there is no reactivity). Europa's circumference, by comparison, is 9.9×10^3 km. Species with high effective sticking coefficients (i.e., high R_{eff}) such as H₂O, H₂O₂, or Na will not travel nearly as far during their lifetime. Although redistribution occurs (e.g., Leblanc and Johnson, 2003), these gas phase species will be more strongly correlated to their source region.

Possible sources for reactivity include sulfur contaminants and broken bonds created by the intense radiation environment. In addition, recent experiments have suggested that O₂ can be trapped as a clathrate by SO₂ and CO₂-containing ice (Hand et al., 2006). Surface reactivity, in the form of a globally uniform O₂ sticking coefficient (e.g., Eviatar et al., 1985; Saur et al., 1998), has been suggested to contribute to oxygen loss, but this would not be able to reproduce the morphology suggested by the HST observations. While sustained exposure to O₂ might be expected to eventually quench the reactivity, intense bombardment by Jupiter's magnetospheric plasma breaks chemical bonds in the surface material providing new opportunities for O₂ to react. The porous regolith also provides a large surface area; for the reasonable assumptions of 100 μm regolith grain radii (spherical grains) and a porosity of 0.9, each 1 cm³ of Europa regolith volume contains ~30 cm² of surface area on the grains. In addition, for the low values of $R_{\text{eff},1}$ used in this paper, O₂ may penetrate deep into the regolith before reacting. Using the Monte Carlo regolith model discussed in Section 4, we found that the average O₂ reaction depth goes from 3.5 cm for $R_{\text{eff},1} = 0.04$ to 21 cm for $R_{\text{eff},1} = 0.01$. While the flux of electron and ion energy is attenuated with depth, energetic electrons travel deeply enough to provide a significant radiation dose at these depths (Cooper et al., 2001). O₂ may also migrate into a regolith grain, especially along internal grain boundaries.

The low column density above the poles appears to require sticking or reactivity comparable to that in the dark terrains. The map we used as a proxy for reactivity did not include the poles. Since there is no reason to believe that the poles have large non-ice contaminant concentrations, the effective reactivity may be due to the significant residence time O₂ has on ice surfaces at low temperatures. Shi et al. (2007) found this time to average about 70 s at 50 K, which is about ten times longer than the residence time at 60 K. The residence time does not directly affect the column densities calculated by our model because, in steady state, the flux adsorbing onto a surface area element is equal to the desorption flux and the time spent on

the surface does not matter. However, significantly increasing the time that an O₂ molecule spends on a regolith grain, as at the poles, can dramatically increase the likelihood of finding a reaction site.

To reproduce the 1999 STIS observation disk-averaged column densities our model requires a larger O₂ source rate ($0.8\text{--}2.0 \times 10^{28}$ O₂ s⁻¹) than typically assumed for Europa (e.g., Paranicas et al., 2002), although it is within the range explored by Saur et al. (1998), Shematovich et al. (2005) and Cooper et al. (2001). Like our model, those models were also constrained by the globally averaged emission rates measured by HST (Hall et al., 1995, 1998). Adding the large loss process that we propose would increase those source rates. The fraction of O₂ lost to surface reactivity in our models, as opposed to loss-to-space processes, is 0.88 for $R_{\text{eff},1} = 0.01$ or 0.96 for $R_{\text{eff},1} = 0.04$. This was, of course, nearly 0 for previous models, although some did include a small sticking coefficient. At Europa, both the relevant laboratory yields and radiation fluxes have considerable uncertainties, and the source rate is highly variable due to temporal variability in the plasma conditions, which might allow for an increased source rate. For instance, the presence of contaminants, such as CO₂, can affect the O₂ production rate (Strazzulla et al., 2005). Another source of uncertainty is the factor $Y_{\text{tot}}(R)/Y(g=0)$ discussed in Section 4, which is not well known for O₂ production. We also note that the modeling of the molecular oxygen atmosphere over Saturn's main rings appeared to require a larger effective source rate than is typically estimated from laboratory data. This might be due to the uncertainties in the measurements and the composition of the ice, but was also attributed in part to the recycling of O on the surfaces of icy grains (Johnson et al., 2006).

As pointed out in the introduction, the spatial morphology of the HST feature in Fig. 1 might be due in part to the spatial distribution of the flow of electrons through Europa's atmosphere which would mitigate the required source rate. Therefore, more observations will be needed to separate the effect of surface reactions from the stimulating radiation flux. Analysis of the New Horizons observations during the Jupiter encounter should be helpful in distinguishing between the spatial morphologies of the atmospheres described here.

Acknowledgments

This work was supported by a NASA Graduate Student Researcher Program fellowship (grant number NNI06AA08H) through NASA's Langley Research Center, a Virginia Space Grant Fellowship, and NASA Planetary Atmospheres grant to R.E.J., PATM NNG06GC09G. M.C.W., R.E.J., and J.F.C. were also supported for the DSMC calculations presented here through an earlier NASA Planetary Atmospheres grant, NASW-02037.

References

- Brown, W.L., Augustyniak, W.M., Marcantonio, K.J., Simmons, E.H., Boring, J.W., Johnson, R.E., Reimann, C.T., 1984. Electronic sputtering of low temperature molecular solids. Nucl. Instrum. Methods Phys. Res. Sect. B Beam Interact. Mater. Atoms 1, 307–314.

- Carlson, R.W., Johnson, R.E., Anderson, M.S., 1999. Sulfuric acid on Europa and the radiolytic sulfur cycle. *Science* 286, 97–99.
- Cassidy, T.A., Johnson, R.E., 2005. Monte Carlo model of sputtering and other ejection processes within a regolith. *Icarus* 176, 499–507.
- Cooper, J.F., Johnson, R.E., Mauk, B.H., Garrett, H.B., Gehrels, N., 2001. Energetic ion and electron irradiation of the icy Galilean satellites. *Icarus* 149, 133–159.
- Domingue, D., Hapke, B., 1992. Disk-resolved photometric analysis of European terrains. *Icarus* 99, 70–81.
- Domingue, D., Verbiscer, A., 1997. Re-analysis of the solar phase curves of the icy Galilean satellites. *Icarus* 128, 49–74.
- Eviatar, A., Bar-Nun, A., Podolak, M., 1985. European surface phenomena. *Icarus* 61, 185–191.
- Fanale, F.P., and 23 colleagues, 1999. Galileo's multiinstrument spectral view of Europa's surface composition. *Icarus* 139, 179–188.
- Hall, D.T., Strobel, D.F., Feldman, P.D., McGrath, M.A., Weaver, H.A., 1995. Detection of an oxygen atmosphere on Jupiter's moon Europa. *Nature* 373, 677–679.
- Hall, D.T., Feldman, P.D., McGrath, M.A., Strobel, D.F., 1998. The far-ultraviolet oxygen airglow of Europa and Ganymede. *Astrophys. J.* 499, 475–481.
- Hand, K.P., Chyba, C.F., Carlson, R.W., Cooper, J.F., 2006. Clathrate hydrates of oxidants in the ice shell of Europa. *Astrobiology* 6, 463–482.
- Hansen, C.J., Shemansky, D.E., Hendrix, A.R., 2005. Cassini UVIS observations of Europa's oxygen atmosphere and torus. *Icarus* 176, 305–315.
- Hapke, B., 1981. Bidirectional reflectance spectroscopy. 1. Theory. *J. Geophys. Res.* 86, 4571–4586.
- Hendrix, A.R., Domingue, D.L., King, K., 2005. The icy Galilean satellites: Ultraviolet phase curve analysis. *Icarus* 173, 29–49.
- Ip, W.H., Williams, D.J., McEntire, R.W., Mauk, B.H., 1998. Ion sputtering and surface erosion at Europa. *Geophys. Res. Lett.* 25, 829–832.
- Johnson, R.E., 1990. *Energetic Charged Particle Interactions with Atmospheres and Surfaces*. Springer-Verlag, New York.
- Johnson, R.E., Lanzerotti, L.J., Brown, W.L., 1982. Planetary applications of ion induced erosion of condensed-gas frosts. *Nucl. Instrum. Methods* 198, 147–157.
- Johnson, R.E., Carlson, R.W., Cooper, J.F., Paranicas, C., Moore, M.H., Wong, M.C., 2004. Radiation effects on the surfaces of the Galilean satellites. In: Bagenal, F., Dowling, T., McKinnon, W. (Eds.), *Jupiter: Satellites, Atmosphere, Magnetosphere*. Cambridge Univ. Press, New York, pp. 483–510.
- Johnson, R.E., and 12 colleagues, 2006. Production, ionization, and redistribution of O₂ in Saturn's ring atmosphere. *Icarus* 180, 393–402.
- Kanik, I., Noren, C., Makarov, O.P., Vattipalle, P., Ajello, J.M., Shemansky, D.E., 2003. Electron impact dissociative excitation of O₂: Absolute emission cross sections of the OI(130.4 nm) and OI(135.6 nm) lines. *J. Geophys. Res.* 108 (E11).
- Kimble, R.A., and 88 colleagues, 1998. The on-orbit performance of the Space Telescope Imaging Spectrograph. *Astrophys. J.* 492, L83–L93.
- Kliore, A.J., Hinson, D.P., Flasar, F.M., Nagy, A.F., Cravens, T.E., 1997. The ionosphere of Europa from Galileo radio occultations. *Science* 277, 355–358.
- Lawrence, G.M., 1970. Dissociative excitation of some oxygen-containing molecules: Lifetimes and electron-impact cross sections. *Phys. Rev. A* 2, 398–407.
- Leblanc, F., Johnson, R.E., 2003. Mercury's sodium exosphere. *Icarus* 164, 261–281.
- Lucchitta, B.K., Soderblom, L.A., 1981. A geologic map of Europa. Reports of Planetary Geology Program—1981, pp. 508–510.
- McEwen, A., 1986. Exogenic and endogenic albedo and color patterns of Europa. *J. Geophys. Res.* B 8, 8077–8097.
- McGrath, M.A., Lellouch, E., Strobel, D.F., Feldman, P.D., Johnson, R.E., 2004. Satellite atmospheres. In: Bagenal, F., McKinnon, W., Dowling, T. (Eds.), *Jupiter: Satellites, Atmosphere, Magnetosphere*. Cambridge Univ. Press, Cambridge, pp. 457–483.
- Nowak, G., Borst, W.L., Fricke, J., 1978. Lifetime determination of the O(⁵S⁰) metastable state via 1356-Å radiation using a time-of-flight technique. *Phys. Rev. A* 17, 1921–1927.
- Paranicas, C., Carlson, R.W., Johnson, R.E., 2001. Electron bombardment of Europa. *Geophys. Res. Lett.* 28, 673–676.
- Paranicas, C., Mauk, B.H., Ratliff, J.M., Cohen, C., Johnson, R.E., 2002. The ion environment near Europa and its role in surface energetics. *Geophys. Res. Lett.* 29 (5), doi:10.1029/2001GL014127.
- Pospieszalska, M.K., Johnson, R.E., 1989. Magnetospheric ion bombardment profiles of satellites: Europa and Dione. *Icarus* 78, 1–13.
- Saur, J., Strobel, D.F., Neubauer, F.M., 1998. Interaction of the jovian magnetosphere with Europa: Constraints on the atmosphere. *J. Geophys. Res.* 103, 19947–19962.
- Shematovich, V.I., Johnson, R.E., Cooper, J.F., Wong, M.C., 2005. Surface-bounded atmosphere of Europa. *Icarus* 173, 480–498.
- Smyth, W.H., Marconi, M.L., 2006. Europa's atmosphere, gas tori, and magnetospheric implications. *Icarus* 181, 510–526.
- Spencer, J.R., Tamppari, L.K., Martin, T.Z., Travis, L.D., 1999. Temperatures on Europa from Galileo PPR: Nighttime thermal anomalies. *Science* 284, 1514–1516.
- Strazzulla, G., Leto, G., LaDelfa, S., Spinella, F., Gomis, O., 2005. Oxidants produced after ion bombardment of water/carbon dioxide icy mixtures. *Mem. Soc. Astron. Ital. Suppl.* 6, 51–56.
- Shi, J., Teolis, B.D., Baragiola, R.A., 2007. Adsorption of O₂ on microporous water ice between 50 and 80 K. *Geophys. Res. Lett.*, submitted for publication.
- Tiscareno, M.S., Geissler, P.E., 2003. Can redistribution of material by sputtering explain the hemispheric dichotomy of Europa? *Icarus* 161, 90–101.